Columnar Mesophase from a New Disclike Mesogen Based on a 3,5-Dicyano-2,4,6-tristyrylpyridine Core

André-Jean Attias,*[,†,‡] Chantal Cavalli,[‡] Bertrand Donnio,[§] Daniel Guillon,[§] Philippe Hapiot,[||] and Jacques Malthête[⊥]

Université Pierre et Marie Curie, UMR 7610, Chimie des Polymères, 4, place Jussieu, Case Courrier 185, F 75252 Paris Cedex 05, France, Département des Matériaux et Systèmes Composites, ONERA, 29, avenue de la Division Leclerc., B.P. 72., F-92322 Châtillon Cedex, France, Groupe des Matériaux Organiques, Institut de Physique et Chimie des Matériaux de Strasbourg, UMR 7504 (CNRS-ULP), 23, rue du Loess, F-67037 Strasbourg Cedex, France, Université de Rennes 1, UMR 6510, Synthèse et Electrosynthèse Organiques, Campus de Beaulieu, F-35042 Rennes Cedex, France, Section de recherche, Institut Curie, UMR 168, 26, rue d'Ulm, F-75248 Paris Cedex 05, France

Received August 9, 2001. Revised Manuscript Received October 17, 2001

We report on the design and synthesis of a new disclike mesogen based on a 3,5-dicyano-2,4,6-tristyrylpyridine core. This compound was characterized by spectroscopic methods (NMR, UV−vis, and photoluminescence) and cyclic voltammetry. The mesogenic behavior was investigated by differential scanning calorimetry, polarized-light optical microscopy, and X-ray diffraction. The disclike structure self-assembles into a hexagonal columnar mesophase and, because of the permanent dipole exhibited by the isolated molecule, the stacking along the columnar axis is antiparallel. Besides two-dimensional charge transfer and fluorescence, the disclike molecule exhibits high electron affinity as a result of the strong acceptor character of the 3,5-dicyanopyridine core.

1. Introduction

Columnar mesophases of disclike mesogens with an extended flat, aromatic, central core have attracted increasing interest as potential one-dimensional conducting systems.[1] Typically, the aromatic cores are stacked one upon another to build columns that are arranged in varied two-dimensional lattices. As the stacking distance is short (3−4 Å) compared to the intercolumnar distance (20−40 Å), electronic interactions within the same column are much stronger than interactions between chromophores in neighboring columns, on one hand, and the large π-overlap of adjacent conjugated aromatic rings allows electrons and excitons migration along the columnar axis,[2] on the other hand. However, short-range order of the intracolumnar stacking and molecular fluctuations within the liquid crystalline phase limit the charge-carrier mobility (10^{-3} cm^2/V·s).[3]

Higher hole mobility values (10^{-1} cm^2/V·s) have been found[4a] in the highly ordered helical columnar (H) phase of 2,3,6,7,10,11-hexahexylthiotriphenylene (HHTT). This enhancement of the electronic properties is explained by the long-range intracolumnar order in the H phase (self-assembled columnar mesophase). Very recently, it was also reported that derivatives of hexabenzocoronene[5] exhibit extremely high charge-carrier mobilities as a consequence of long-range order in a room-temperature hexagonal columnar mesophase.

These high electronic properties associated with long-range columnar order make discotic liquid crystals promising as organic semiconductors for applications in the domain of molecular electronics and optoelectronics,[4−7] more particularly, in the area of photocon-

* To whom correspondence should be addressed. Tel.: (+33) 1 44 27 53 02. Fax: (+33) 1 44 27 70 89. E-mail: attias@ccr.jussieu.fr.
† Université Pierre et Marie Curie.
‡ ONERA.
§ Institut de Physique et Chimie des Matériaux de Strasbourg.
|| Université de Rennes 1.
⊥ Institut Curie.

(1) (a) *Handbook of Liquid Crystals*; Demus, D., Goodby, J., Gray, G. W., Spiess, H.-W., Vill, V., Eds.; Wiley-VCH: Weinheim, 1998; Vol. 2b. (b) For references see: Van de Craats, A. M.; Warman, J. M. *Adv. Mater*. **2001**, *13*, 130.

(2) (a) Mertesdorf, C.; Ringsdorf, H.; Stumpe, J. *Liq. Cryst*. **1991**, *9*, 337. (b) Marguet, S.; Markovitsi, D.; Millié, P.; Sigal, H.; Kumar, S. *J. Phys. Chem. B* **1998**, *102*, 4697. (c) Markovitsi, D.; Germain, A.; Millié, P.; Lecuyer, P.; Gallos, L. K.; Argyrakis, P.; Bengs, H.; Ringsdorf, H. *J. Phys. Chem*. **1995,** *99*, 1005. (d) Markovitsi, D.; Gallos, L. K.; Lemaistre, J. P.; Argyrakis, P. *Chem. Phys.* **2001**, *269*, 147.

(3) (a) Adam, D.; Closs, F.; Frey, T.; Funhoff, D.; Haarer, D.; Ringsdorf, H.; Schuhmacher, P.; Siemensmeyer, K. *Phys. Rev. Lett.* **1993**, 70, 457. (b) Bässler, H. *Adv. Mater*. **1993**, *5*, 662. (c) Bässler, H.; Borsenberger, P. M. *Chem. Phys*. **1993**, *177*, 662.

(4) (a) Adam, D.; Schuhmacher, P.; Simmerer, J.; Haüssling, L.; Siemensmeyer, K.; Etzbach, K. H.; Ringsdorf, H.; Haarer, D. *Nature* **1994**, *371*, 141. (b) Adam, D.; Schuhmacher, P.; Simmerer, J.; Haüssling, L.; Paulus, W.; Siemensmeyer, K.; Etzbach, K.-H.; Ringsdorf, H.; Haarer, D. *Adv. Mater*. **1995**, *7*, 276. (c) Simmerer, J.; Glüsen, B.; Paulus, W.; Kettner, A.; Schuhmacher, P.; Adam, D.; Etzbach, K.-H.; Siesmensmeyer, J.; Wendorff, J. H.; Ringsdorf, H.; Haarer, D. *Adv. Mater*. **1996**, *8*, 815. (d) Van de Craats, A. M.; Warman, J. M.; De Haas, M. P.; Adam, D.; Simmerer, J.; Haarer, D.; Schuhmacher, P. *Adv. Mater*. **1996**, *8*, 823.

(5) (a) Van de Craats, A. M.; Warman, J. M.; Müllen, K.; Geerts, Y.; Brand, J. D. *Adv. Mater.* **1998**, *10*, 36. (b) Van de Craats, A. M.; Warman, J. M.; Fechtenkötter, A.; Brand, J. D.; Harbison, M. A.; Müllen, K. *Adv. Mater.* **1999**, *11*, 1469.

(6) (a) Liu, C.-Y.; Pan, H.-L.; Fox, M. A.; Bard, A. J. *Science* **1993**, *261*, 897. (b) Petritsch, K.; Friend, R. H.; Lux, A.; Rozenberg, G.; Moratti, S. C.; Holmes, A. B. *Synth. Met***. 1999**, *102*, 1776.

10.1021/cm010725h CCC: $22.00
Published on Web 12/18/2001

Scheme 1

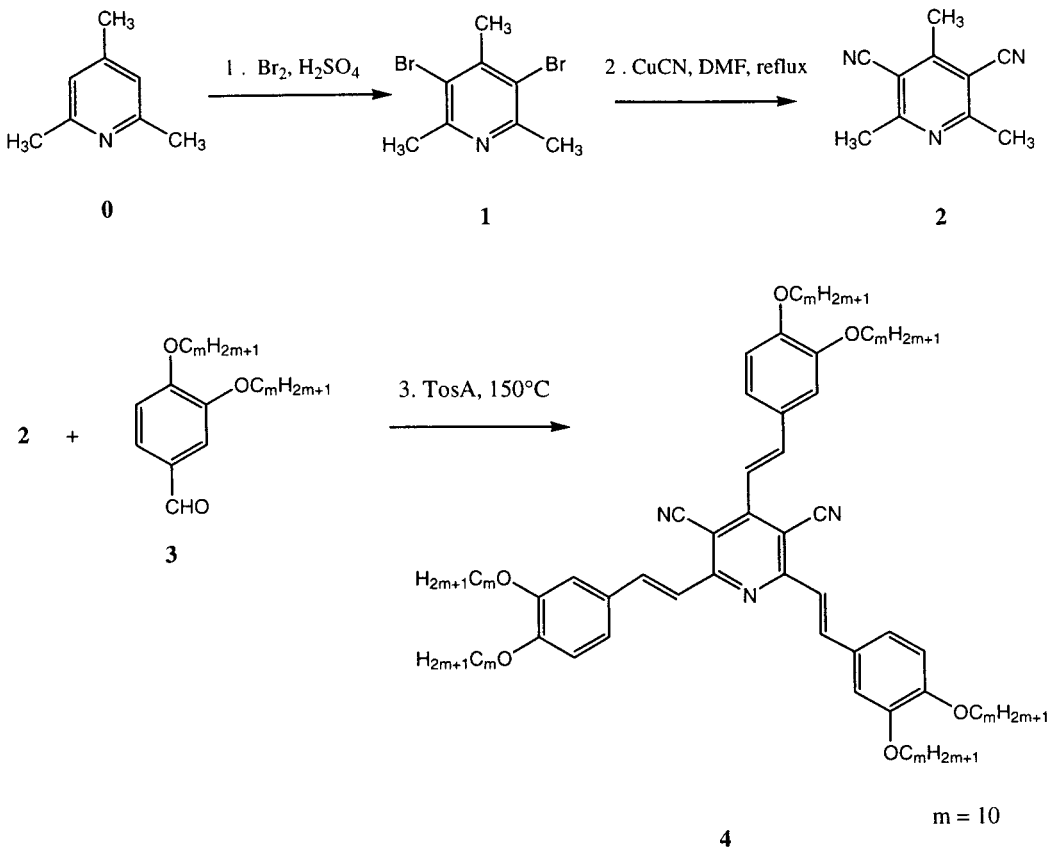

ductivity[4] and for photovoltaic[6] and electroluminescent devices.[7]

In this context we were interested in designing and synthesizing a new class of columnar disclike liquid-crystal molecules (i) with high electron affinity to favor electrons injection and (ii) based on a core having a permanent electric dipole perpendicular to the column axis to favor strong dipolar interactions and consequently long-range intracolumnar order. It should be noted that only a few examples of the induction of columnar mesophases by either disclike molecules with a dipolar nature[8] or nondiscoid polar molecules such as noncentrosymmetric polarizable rodlike molecule,[9] half-disc-shaped metallomesogens,[10] or bent-rod hexacatenar mesogens[11] have been reported.

In previous papers[12,13] we presented a strategy to synthesize by means of the Knoevenagel condensation a series of 6,6′-distyryl-3,3′-bipyridine derivatives as a new class of rodlike liquid-crystalline conjugated molecules. These compounds were prepared by reaction of 6,6′-dimethyl-3,3′-bipyridine with aromatic aldehydes. They exhibit, in addition to mesomorphism, (i) NLO properties,[13] (ii) intense fluorescence associated with high electron affinity,[12b] properties that open up light-emitting diodes (LEDs) applications.

In the present work, we report the first results on the synthesis and characterization of a new disclike molecule, the 3,5-dicyano-2,4,6-tris(3,4-didecyloxystyryl)-pyridine (**4**) (Scheme 1). 3,5-Dicyano-2,4,6-trimethylpyridine (**2**) has been chosen as the starting material, the 3,5-dicyanopyridine structure acting as an acceptor core, because the pyridine is an electron-deficient aromatic heterocycle with a localized lone pair of electrons in an sp^2 orbital on the nitrogen atom on one hand and is substituted by two cyanide groups on the other one. Moreover, **2** has a permanent dipole because the two cyanide groups are at the 3 and 5 positions of the pyridine ring. According to the synthetic strategy described, **2** results, when reacting with aromatic aldehydes bearing electron-donor groups (**3**), in a highly π-conjugated molecule, **4**, which possesses also a permanent dipole and is a two-dimensional intramolecular charge-transfer system as illustrated in Scheme 2. It is of interest to note that this latter characteristic induces planarity, a factor that is favorable to liquid crystallinity. However, it should be noted that the length of the additional alkyl chains ($m = 10$) was not optimized. Compound **4** was characterized by means of ^1H and ^{13}C NMR spectroscopies, elemental analysis, differential scanning calorimetry (DSC), polarized-light optical mi-

(7) (a) Christ, T.; Glüsen, B.; Greiner, A.; Kettner, A.; Sander, R.; Stümpflen, V.; Tsukruk, V.; Wendorff, J. H. *Adv. Mater.* **1997**, *9*, 48. (b) Bacher, A.; Bleyl, I.; Erdelen, C. H.; Haarer, D.; Paulus, W.; Schmidt, H.-W. *Adv. Mater.* **1997**, *9*, 1031. (c) Seguy, I.; Destruel, P.; Bock, H. *Synth. Met.* **2000**, *111*−*112*, 15. (d) Hassheider, T.; Benning, S. A.; Kitzerow, H.-S.; Achard, M.-F, Bock, H. *Angew. Chem., Int. Ed.* **2001**, *40*, 2060. (e) Seguy, I.; Jolinat, P.; Destruel, P.; Farenc, J.; Mamy, R.; Bock, H.; Ip, J.; Nguyen, T. P. *J. Appl. Phys.* **2001**, *89*, 5442.

(8) Pucci, D.; Veber, M.; Malthête, J. *Liq. Cryst.* **1996**, *21*, 153.

(9) Paulus, W.; Ringsdorf, H.; Diele, S.; Pelzl, G. *Liq. Cryst.* **1991**, *9*, 807.

(10) Trzaska, S. T.; Swager, T. M. *Chem. Mater.* **1998**, *10*, 438, and references therein.

(11) Levitsky, A. I.; Kishikawa, K.; Eichhorn, S. H.; Swager, T. M. *J. Am. Chem. Soc.* **2000**, *122*, 2474.

(12) (a) Attias, A.-J.; Cavalli, C.; Bloch, B.; Guillou, N.; Noël, C. *Chem. Mater.* **1999**, *11*, 2057. (b) Attias, A.-J.; Hapiot, P.; Wintgens, V.; Valat, P. *Chem. Mater.* **2000**, *12*, 461.

(13) (a) Lemaître, N.; Attias, A.-J.; Ledoux, I.; Zyss, J. *Chem. Mater.* **2001**, *13*, 1420. (b) Chérioux, F.; Attias, A.-J.; Maillotte, H. submitted to *Adv. Funct. Mater.*

Scheme 2

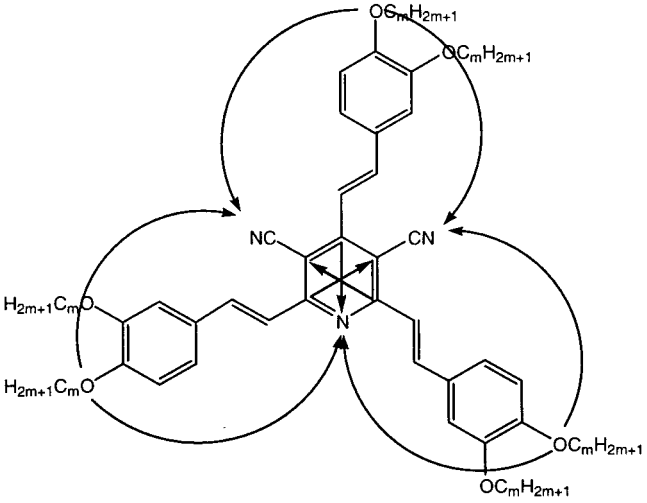

croscopy (POM), X-ray diffraction (XRD), cyclic voltammetry, and UV/visible and fluorescence spectroscopies in solution. Specific properties that are of interest are (i) the changes in the thermal transitions and liquid-crystalline behavior, (ii) redox potential (used to estimate the relative ionization potential and electron affinity), and (iii) optical properties (absorption and emission spectra in solution, Stokes shift, and emission quantum yield).

2. Experimental Section

2.1. Techniques. 2.1.1. Nuclear Magnetic Resonance (NMR) Spectroscopy. ^{1}H and ^{13}C NMR spectra were recorded on a Varian Unity 300 spectrometer operating at 299.95 and 75.144 MHz, respectively. Chloroform-*d* ($CDCl_3$) was used as the solvent and tetramethylsilane (TMS) as the internal standard.

2.1.2. Thermal Analysis. DSC thermograms were recorded on a Perkin-Elmer DSC 7 instrument, at a scanning rate of 5 °C min^{-1}.

2.1.3. Phase Behavior. Textures were observed on a Leitz Ortholux polarizing optical microscope equipped with a Mettler FP 82 heating stage attached with a Mettler FP 80 temperature controller.

2.1.4. X-ray Diffraction (XRD). The XRD patterns were obtained with two different experimental setups, and in all cases, the crude powder was filled in Lindemann capillaries of 1-mm diameter. A linear monochromatic Cu Kα_1 beam (λ = 1.5405 Å) obtained with a sealed-tube generator (900 W) and a bent quartz monochromator were used. One set of diffraction patterns was registered with a curved counter Inel CPS 120. In this setup, the exposure time was 1 h, every 10 °C. The sample temperature was controlled within ±0.5 °C; periodicities up to 60 Å can be measured. The other set of diffraction patterns was registered on an Image Plate; the cell parameters were calculated from the position of the reflection at the smallest Bragg angle, which is in all cases the most intense. Periodicities up to 90 Å can be measured, the sample temperature was controlled within ±0.3 °C, and the exposure times were varied between 24 and 72 h.

2.1.5. Cyclic Voltammetry. Electrochemistry experiments were performed with a three-electrode setup using a platinum counter electrode and a reference electrode. The reference electrode was an aqueous saturated calomel electrode with a salt bridge containing the supporting electrolyte. The working electrode was either discs of glassy carbon (∅ 0.8 mm, Tokai Corp.), gold (∅ 1 mm), or platinum (∅ 1 mm). The working electrodes were carefully polished before each set of voltammograms with 1-μm diamond paste and cleansed in an ultrasonic bath with dichloromethane. The electrochemical instrumentation consisted of a PAR Model 175 Universal programmer and of a home-built potentiostat equipped with a positive feedback compensation device.[14] The data were acquired with a 310 Nicolet oscilloscope. The potential values were internally calibrated against the ferrocene/ferricinium couple ($E° = 0.405$ V vs SCE) for each experiment. All the cyclic voltammetry experiments were carried out at 20 °C using a cell equipped with a jacket, allowing circulation of water from the thermostat. Oxygen was removed from all solutions by bubbling argon. The solvent was a toluene/acetonitrile mixture (50/50 v/v) and the supporting electrolyte was tetrabutylammonium tetrafluoroborate (Fluka, Puriss) at a concentration of 0.1 mol·L^{-1}. Acetonitrile was from Merck (Uvasol quality <0.01% of water) and toluene from Prolabo (R.P. Normapur).

2.1.6. Optical Spectroscopies. The UV−visible absorbance spectrum was recorded using a Lambda 18 UV/vis spectrometer (Perkin-Elmer). A 1-cm quartz cell was used. The concentration was chosen so that an appropriate absorbance value (0.1−0.2) was obtained at λ_{max}. The fluorescence and excitation spectra were obtained from the same solution, using an Aminco S.L.M. 8100 luminescence spectrometer. The fluorescence quantum yield was measured in toluene/acetonitrile (50/50 v/v) solution by comparison with the emission of quinine sulfate for which a value of 0.55 has been taken.[15] The quantum yield was not corrected for the change in refractive index between the CH_2Cl_2 solution and aqueous sulfuric solution.

2.2. Reagents. 2,4,6-Trimethylpyridine (2,4,6-collidine), bromine, copper cyanide, 3,4-dihydroxybenzaldehyde, 1-bromodecane, and *p*-toluenesulfonic acid monohydrate (all from Aldrich) were used without further purification. Sulfuric acid was purchased from Merck.

2.3. Syntheses. 2.3.1. 3,5-Dibromo-2,4,6-trimethylpyridine (1). A 500-mL three-necked flask fitted with a reflux condenser, a dropping funnel, and an argon inlet was charged with 2,4,6-trimethylpyridine (60.5 g, 0.5 mol). The solution was cooled and treated at ice-bath temperature with 25 mL of fuming sulfuric acid (65% oleum) added dropwise. When the temperature of the solution was stable, indicating the neutralization of the 2,4,6-trimethylpyridine, excess of fuming sulfuric acid (275 mL) was added. Then, the resulting solution was warmed to 90 °C, bromine (25.8 mL, 0.5 mol) was added dropwise, and the resulting mixture was stirred at reflux (oil bath, 80 °C) under argon for 24 h. After cooling to room temperature, the reaction mixture was poured into an ice-bath and neutralized by washing with a 5 N sodium hydroxide solution. The beige precipitate was isolated by filtration and purified by crystallization from an ethanol−water (1:1) solution. Finally, 114.4 g (0.41 mol) of 3,5-dibromo-2,4,6-trimethylpyridine was obtained as a gray powder (yield: 82%). ^{1}H NMR ($CDCl_3$) δ [ppm]: 2.589 (s, 3H), 2.604 (s, 6H). ^{13}C NMR ($CDCl_3$) δ [ppm]: 24.66, 25.42, 121.26, 146.88, and 154.83. Anal. Calcd for $C_8H_9NBr_2$: C, 34.41; H, 3.23; N, 5.02. Found: C, 34.61; H, 3.28; N, 4.98.

2.3.2. 3,5-Dicyano-2,4,6-trimethylpyridine (2). 3,5-Dibromo-2,4,6-trimethyl-pyridine (12.8 g, 0.045 mol), copper cyanide (10 g, 0.142 g), and *N*,*N*-dimethylformamide (40 mL) were refluxed for 6 h while being stirred. The reaction mixture was poured, while stirring, into 400 mL of cold water. The precipitate was collected and washed successively with water, warm aqueous sodium cyanide (10%, 150 mL), and then water. The resulting brown product was extracted four times with dichloromethane (4 × 120 mL). Finally, after the removal of the solvent, 6.18 g (0.036 mol) of 3,5-dicyano-2,4,6-trimethylpyridine was obtained as a brown powder (yield: 79%). ^{1}H NMR ($CDCl_3$) δ [ppm]: 2.70 (s, 3H), 2.76 (s, 6H). ^{13}C NMR ($CDCl_3$) δ [ppm]: 19.8, 24.4, 108.3, 114.7, 145.9, and 164.3. Anal. Calcd for $C_{10}H_9N_3$: C, 70.71; H, 5.41; N, 24.39. Found: C, 70.16; H, 5.3; N, 24.54.

(14) Garreau, D.; Savéant, J.-M. *J. Electroanal.* **1972**, *35*, 309.
(15) Melhuish, W. H. *J. Phys. Chem.* **1961**, *65*, 229.

Table 1. Thermodynamic Data and Phase Sequence of 4

phase − *transition temperature (°C)* − [enthalpy changes ΔH (kJ·mol^{-1})][a]	
1st heating	1st cooling
M_1 *60.0* [∼36] **X** *70.5* [∼−4] **M_2** *74.0* [∼19] **Col_H** *133.5* [2.2] **I**	**I** *133.5* [−1.5] **Col_H** *61.0* [−6.3] **M_3**

[a] Determined by DSC. M_1, M_2, and M_3: see text; Col_H: hexagonal columnar mesophase; X: exothermic peak; I: isotropic phase.

2.3.3. 3,4-Didecyloxybenzaldehyde (3). 3 was prepared by adapting literature procedures.[16]

2.3.4. 3,5-Dicyano-2,4,6-tris(3,4-didecyloxystyryl)pyridine (4). A 50-mL three-necked round-bottom flask equipped with a reflux condenser, a dropping funnel, and an argon inlet was charged with 3,5-dicyano-2,4,6-trimethylpyridine (750 mg, 4.38 mmol), 3,4-didecyloxybenzaldehyde (7.14 g, 17.1 mmol), and *p*-toluenesulfonic acid monohydrate (510 mg, 2.7 mmol). The reaction mixture was then warmed to 150 °C, stirred for 7 h under argon, and cooled to room temperature. The resulting mixture was poured into 100 mL of a 2 N hydroxide sodium solution and extracted with dichloromethane (3 × 150 mL). The combined organic phases were washed with water, dried over $MgSO_4$, and concentrated to obtain a brown solid. The crude product was crystallized from hot ethanol and three times from hexane to yield 2.52 g (1.8 mmol) of 3,5-dicyano-2,4,6-tris(3,4-didecyloxystyryl)pyridine as a yellow-orange solid (yield: 42%). ^{1}H NMR ($CDCl_3$) δ [ppm]: 0.88 (m, 18H), 1.28 (m, 84H), 1.80 (m, 12H), 4.05 (m, 12H), 6.89 (d, 1H, ^3J(H,H) = 8.36 Hz), 6.90 (d, 2H, ^3J(H,H) = 8.36 Hz), 7.2 (m, 7H), 7.41 (d, 2H, ^3J(H,H) = 15.55 Hz), 7.87 (d, 1H, ^3J(H,H) = 16.12 Hz), and 8.15 (d, 2H, ^3J(H,H) = 15.55 Hz). ^{13}C NMR ($CDCl_3$) δ [ppm]: 14.14, 22.71, 26.03, 26.09, 29.15, 29.19, 29.3, 29.38, 29.44, 29.49, 29.61, 29.65, 31.9, 69.08, 69.5, 101.37, 112.45, 112.80, 113.00, 113.10, 116.38, 118.08, 120.32, 122.35, 122.86, 127.91, 128.28, 141.20, 142.08, 149.28, 149.35, 151.49, 151.60, 152.09, 159.45. Anal. Calcd for $C_{91}H_{144}N_3O_6$: C, 79.60; H, 10.35; N, 3.06; O, 6.99. Found: C, 79.68; H, 10.54; N, 3.02; O, 6.76.

3. Results and Discussion

3.1. Synthesis. Scheme 1 outlines the overall pathway of preparing 3,5-dicyano-2,4,6-tris(3,4-didecyloxystyryl)pyridine (**4**). This compound was synthesized in three steps from collidine (**0**). Bromation of collidine with a slight excess of elemental bromine afforded the 2,4,6-tristyryl-3,5-dibromopyridine (**1**), which was converted into the 3,5-dicyano derivative (**2**) in the presence of copper cyanide.[17] The overall yield for the conversion of **0** to **2** was ≈65%. Toluenesulfonic-acid-catalyzed Knoevenagel-type condensation of **2** with 3 equiv of **3** afforded the resulting 3′,4′-didecyloxy-2,4,6-tristyryl-3,5-dicyanopyridine, which was isolated in 42% yield as a yellow-orange powder.

The structure and purity of all the compounds were confirmed by using ^{1}H NMR, ^{13}C NMR, and elemental analyses. The ^{1}H and ^{13}C NMR spectra of **1**, **2**, and **4** were consistent with the proposed structure. Thus, the remaining resonances at 2.76 and 2.70 ppm in the ^{1}H NMR spectrum of **2** correspond to the methyl protons at the 2 and 4 positions, respectively, of the pyridine ring. The resonances of the corresponding carbons are observed at 24.40 and 19.80 ppm in the ^{13}C NMR spectrum, while the resonances at 114.7 ppm, on one hand, at 108.3, 154.9, and 164.3, on the other hand, are attributed to the carbons of the cyano groups and at the 3 (5), 4, and 2 (6) positions of the pyridine ring, respectively. The ^{1}H NMR spectrum of **4** is equally consistent with the proposed structure. Indeed, (i) there is a complete disappearance of the methyl protons present in **2,** (ii) two doublets appear at 8.15 and 7.87 ppm with a three-bond coupling constant $^3J_{H,H}$ = 15.55 and 16.12 Hz respectively, indicative of a trans carbon−carbon double bond. These resonances are assigned to the two kinds of trans vinylene units at the 2 (6) and 4 positions of the pyridine ring, respectively. In addition, the ratio of the integrated aromatic resonances versus the aliphatic ones is equal to 15/44 as expected. Moreover, the elemental analysis data of **1**, **2**, and **4** show good agreement with the proposed structures.

3.2. Mesomorphic Behavior. The thermal behavior of compound **4** was examined by DSC and phase assignments were based on powder X-ray diffraction (XRD) and polarized-light optical microscopy (POM). The transition temperatures, phase sequence, and some thermodynamic data are listed in Table 1.

Placed between glass and a cover slide, **4** displays a surprisingly perfect homeotropic alignment in the mesomorphic state, upon heating from 78.5 to 135 °C, and thus it appears black between crossed polarizers: the orientational director of the molecular discs, that is, the column axis, is perpendicular to the substrate surface. So to avoid this orientation, which does not allow one to observe liquid-crystalline textures, the sample was mounted between two glass slides, which were modified with an alkoxysilane (octadecyltrichlorosilane) usually used to induce an alignment of the liquid-crystal chains perpendicular to the surface substrate. A beautiful fan-shaped texture, characteristic of a hexagonal columnar mesophase, is obtained in that case as evidenced in Figure 1. Upon further heating, the sample clears directly into the isotropic liquid without showing additional mesophase.

During the first heating, and prior to the melting into the columnar mesophase at 78.5 °C, the DSC traces (Figure 2a) showed complex thermal behavior. A first broad endothermic peak at 67 °C (onset at 60 °C, $\Delta H \sim$ 36 kJ·mol^{-1}), corresponding to the melting of the starting material M_1 (see Table 1), was followed by an exothermic event ($\Delta H \sim -4$ kJ·mol^{-1}) at 70.5 °C, which corresponds to crystallization into another crystalline phase, M_2. This second phase then immediately melted into the liquid-crystalline phase at 78.5 °C (onset at 74 °C, $\Delta H \sim$ 19 kJ·mol^{-1}). At 133.5 °C (onset 133.5 °C, ΔH = 2.2 kJ·mol^{-1}), the mesophase clears into the isotropic liquid. No peak corresponding to another eventual mesophase, such as a nematic phase, was detected on the DSC traces in this temperature range (78−133 °C) or above. Moreover, upon cooling (Figure 2b), the isotropic liquid-to-mesophase transition was seen at 133 °C (onset 133.5 °C, $\Delta H = -1.5$ kJ·mol^{-1}), showing a weak hysteresis. Upon further cooling, a monotropic transition was also observed at 61 °C ($\Delta H = -6.3$ kJ·mol^{-1}). Then, upon heating, just after reaching 45

(16) For example: Donnio, B.; Heinrich, B.; Gulik-Krzywicki, T.; Delacroix, H.; Guillon, D.; Bruce, D. W. *Chem. Mater.* **1997**, *9*, 2951.
(17) Friedman, L.; Shechter, H. *J. Org. Chem.* **1961**, *26*, 2522.

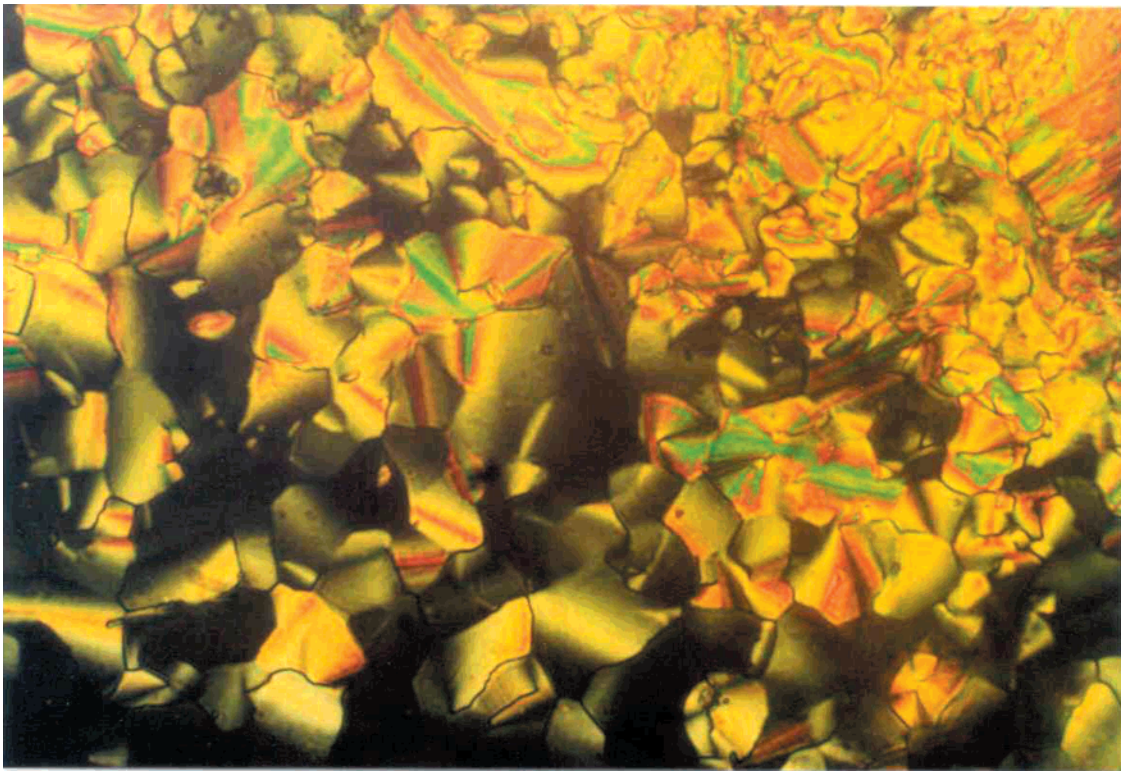

Figure 1. Optical texture of **4** mounted between alkoxysilane-modified slides. The photomicroscopic picture of the mesophase was obtained with a polarizing microscope upon cooling from the isotropic liquid at 80 °C (crossed polarizers).

°C, the same transition occurred at 63 °C (ΔH = 7.1 kJ·mol^{-1}). Both weak hysteresis and enthalpy suggest the presence of a metastable mesophase M_3 below the columnar mesophase. Upon subsequent heating−cooling cycles, the first peak occurred at 81 °C, while both Col_H−I and Col_H−M_3 transitions showed excellent reproducibility.

Temperature-dependent X-ray diffraction (XRD) measurements were carried out every 10 °C starting in the solid state at 30 °C up to 160 °C in the isotropic liquid and the evolution of the X-ray diffractograms with temperature is reported in Figure 3a. Good agreement was found between the transition temperatures derived from both POM and DSC techniques with those determined by XRD (the slight shifts in temperatures are due to different calibration methods, and experiments for DSC, POM, and XRD; see Experimental Section). Four different temperature domains were identified for which representative X-ray patterns (A, B, C, and D, respectively) are reported in Figure 3a. The first one is comprised between room temperature and ≈60 °C. Its associated X-ray diffractogram (A) is characterized by the presence of a broad and diffuse peak of weak intensity in the small angle area, and of another broad scattering in the wide angle region; thus, M_1 (see Table 1) is either an amorphous solid or a noncrystallized solid.[18] A further increase of the temperature up to 80 °C results in a transformation of the X-ray patterns: the representative X-ray pattern B shows a series of discrete and sharp small angle reflections (e.g., at 80 °C; 29.4 and 25.8 Å for the two most intense reflections at the smallest angles) and additional small reflections appear in the wide angle region. Despite the large number of reflections, the nature of the associated M_2 phase could not be assigned, that is, the reflections could not be indexed in any of the 2D space groups associated to columnar mesophases. Such features nevertheless suggest either a disordered solid or an ordered liquid-crystalline phase (positional order, but no orientational order). Note that the complex behavior seen by DSC could not be reproduced here; this is due to the two different setups and to the change of the kinetics of the system. Then, in the temperature range 80−135 °C, the X-ray patterns (C) revealed the existence of a third zone attributed to a liquid-crystalline mesophase, as hereunder detailed. Finally, a further increase in temperature, above 135 °C, results in a transformation of the X-ray diffractogram (D) characterized by the collapse of the intense reflection into a large peak (corresponding roughly to the molecular dimensions) and to the flattening of the diffuse wide-angle halo, confirming that the mesophase has cleared into the isotropic liquid consistent with DSC and POM observations. This pattern remained identical at 140, 150, and 160 °C, indicating that some molecular clusters are still present, although not correlated to each other, in the liquid phase, high above the clearing point. Upon cooling, almost the same evolution of the X-ray diffractograms was observed (E and F). At 60 °C, one can see the development of some ordering in the mesophase revealed by the presence of small peaks appearing in the small angle region, and of a well-defined peak at 3.5 Å, besides the wide angle halo at 4.5 Å: the X-ray diffractogram E corresponds to an intermediate state between the ones associated to X-ray patterns C and B and is very likely associated to the formation of the metastable

(18) Guinier, A. In *La Structure de la Matière*; Hachette-CNRS Ed.: Paris, 1980; Chapter 8−9; pp 203−258.

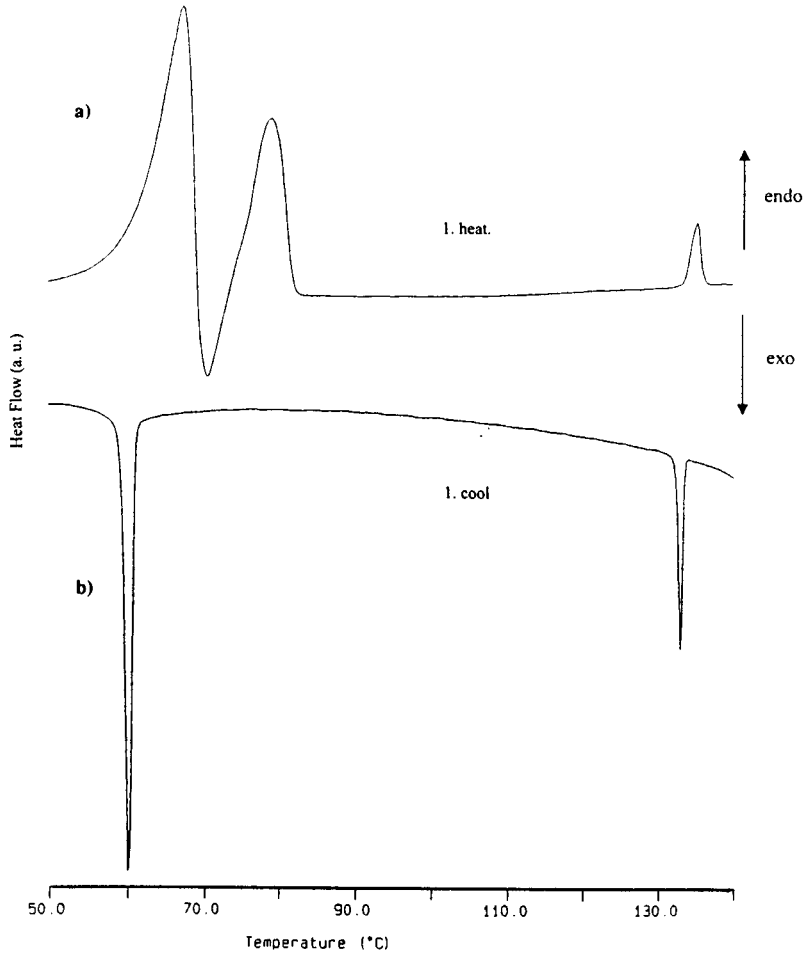

Figure 2. DSC traces for **4** upon (a) heating and (b) cooling (scan rate 5 °C min^{-1}).

pseudo-crystalline mesophase M_3. Upon further cooling, the X-ray diffractogram E is tranformed into the F one, similar to the A one: the initial noncrystallized solid M_1 is reformed, although no transition was detected by DSC, confirming that, in this system, M_3 is the kinetically stable phase, while M_1 is the thermodynamically stable one.

Figure 3b shows a representative X-ray diffractogram of the mesophase recorded at 100 °C. The pattern consists of (i) a broad diffuse scattering halo (**II**) in the wide angle region, corresponding to the liquidlike disorder of the aliphatic chains, at ≈4.5 Å, (ii) another broad diffuse band (**III**) at ≈3.5 Å, which is a characteristic distance usually found between flat aromatic cores (and corresponding to the stacking period in a column[19]), (iii) a third less intense broad band (**I**) at ≈7.1 Å, which may be an indication of some "dimerization", resulting from an antiparallel stacking of the molecules[10] (the double of **III**), and finally (iv) a single sharp and intense reflection (27.1 Å) in the small angle region. Identical X-ray patterns were obtained at all other temperatures of the mesomorphic range, with no change of position of the fundamental reflection.

Such features are not totally conclusive to determine the real nature of the mesophase. However, three facts strongly suggest that the mesophase is columnar hexagonal (Col_H). First, the disclike structure of the molecules must lead preferably to the formation of columns, and thus of columnar phases, by their long range order stacking rather than to layered structures or nematic arrangements. Such stacking is also facilitated by the antiparallel arrangement of the molecular dipoles (estimated at 3.9 D by means of a calculation on the AM1-optimized geometry[20]) as sketched in Figure 4a and confirmed by the presence of the diffuse halos **I** and **III**.[10] In such configuration, the alkyl chains fill the void between the rigid branches in a more efficient manner. Second, the observation of the optical texture by POM revealed characteristic defects of a Col_H phase, namely, the formation of a fan-shaped texture (Figure 1), and the strong tendency for homeotropic alignment. Third, because only one fundamental Bragg reflection was observed, which is on the order of magnitude (27.1 Å) of the molecular dimension, the 2D rectangular and oblique lattices are excluded, as only one single intense reflection was observed in the small angle region, leaving the hexagonal packing symmetry as the unique possibility;[19] the apparent broadness of the base of this reflection is due to the diffusion of the air. Thus, the structural parameters of the Col_H mesophase (Figure 4b), that is, the columnar repeat distance *h* and the first-

(19) (a) Destrade, C.; Tinh, N. G.; Gasparoux, H.; Malthête, J.; Levelut, A. M. *Mol. Cryst. Liq. Cryst.* **1981**, *71*, 111. (b) Levelut, A. M. *J. Chim. Phys.* **1983**, *80*, 149. (c) Guillon D. *Struct. Bond.* **1999**, *95*, 41.

(20) (a) Calculations were performed using the PC-Spartan software 1.1 (Wavefunction Inc, Irvine, CA). (b) diameter $\phi_0 = 2 \times$ (radius taken from the center of the pyridine ring to the oxygen atom position).

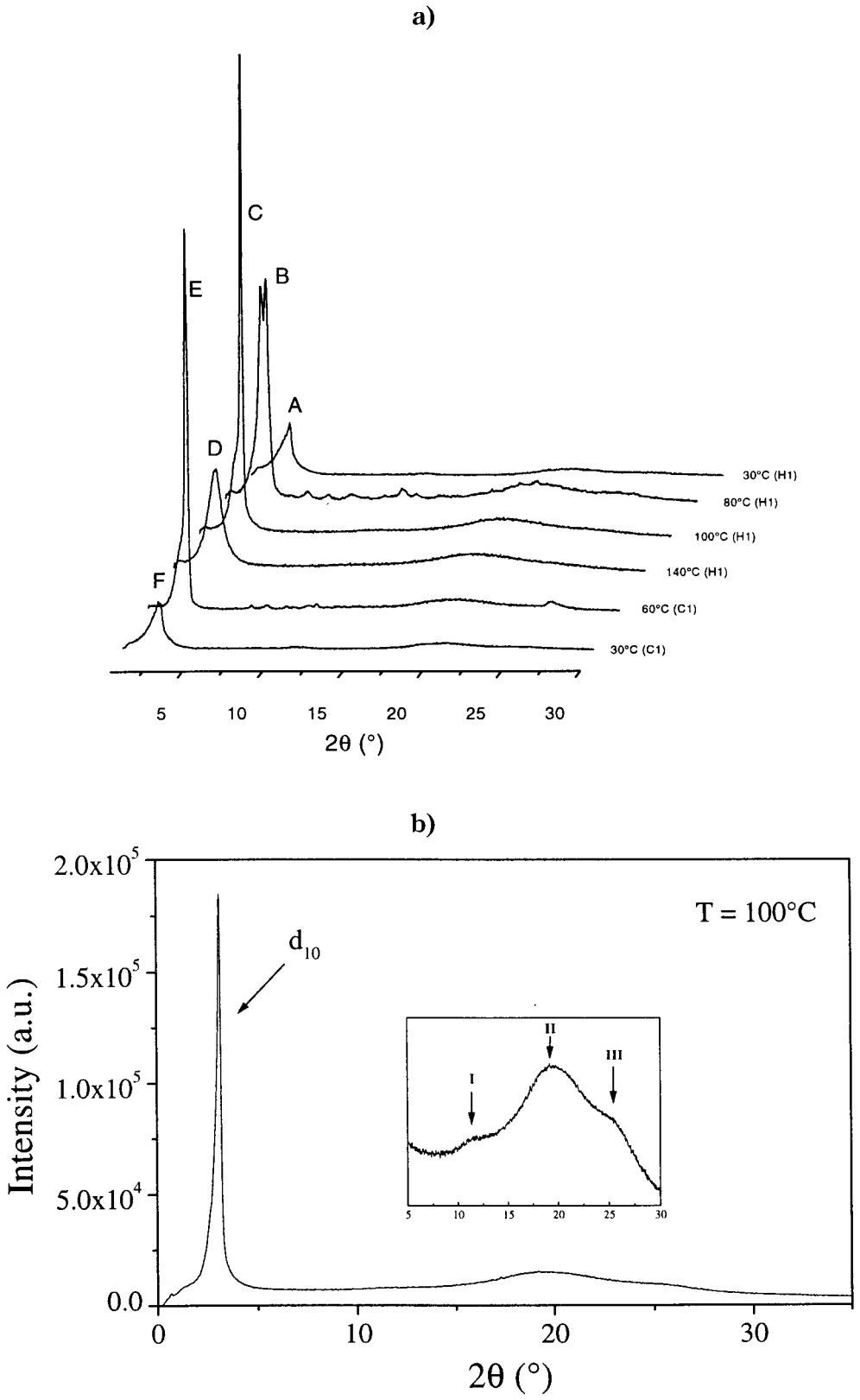

Figure 3. X-ray diffraction patterns of **4**: (a) temperature dependence upon first heating (H1) and first cooling (C1); (b) in the mesophase at 100 °C.

order spacing d_{10}, are equal to 3.5 Å (estimated from the center position of the halo **III)** and 27.1 Å, respectively. The molecular diameter of the hard disclike core ϕ_{Ar} (without the aliphatic chains) has been estimated at 18.7 Å by means of a calculation on the AM1-optimized geometry.[20b] The complete thermal behavior of **4** is summarized in Table 1.

To obtain more insights of the molecular arrangement inside the column, the number of molecules N_{Mol} contained in each columnar slice 3.5-Å thick and the cross-

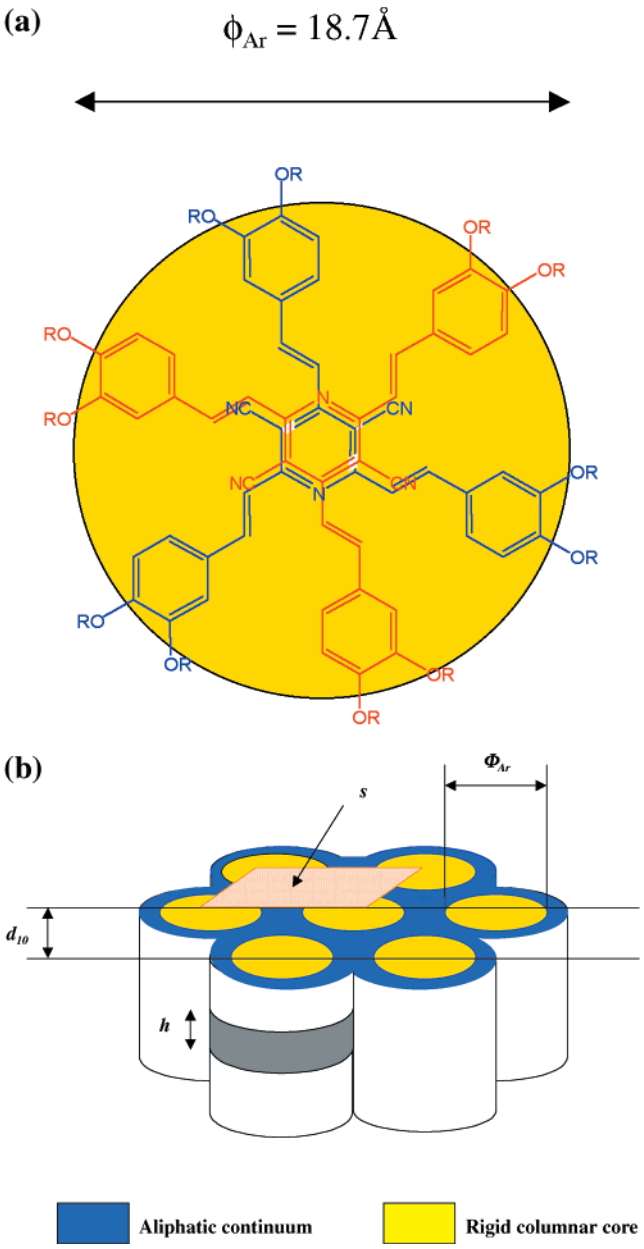

Figure 4. (a) Schematic representation of the disc-shaped structure formed with the dimer of **4**. ϕ_{Ar} is the diameter of the dimer's aromatic part. (b) Schematic representation of the hexagonal columnar lattice. Structural parameters *h*, *s*, and d_{10} are discussed in the text.

sectional area of the inner rigid part of the column, s_{Ar}, have been evaluated.

N_{Mol} can be calculated by using the following equation,

$$N_{Mol} = \frac{hs}{V_{Mol}} = \frac{2d_{10}^{2}}{\sqrt{3}} \frac{h}{V_{Mol}} \qquad (1)$$

where *h* and d_{10} refer to the average columnar repeat unit distance and to the first-order columnar spacing, respectively, both values being determined by X-ray diffraction, *s* corresponds to the cross section of the hexagonal columnar phase as defined in Figure 4b ($s = (2/\sqrt{3})d_{10}^{2}$)[16], and V_{Mol} is the molecular volume[16] (at 100 °C, h = 3.5 Å, d_{10} = 27.1 Å, s = 848 Å^2, and V_{Mol} = 2540 Å^3).[21] The calculation results in $N_{Mol} \sim 1.17$, showing that, on average, about one molecule is needed to fill such a columnar slice.

The symmetry of the columnar lattice being hexagonal, the hard columnar core (i.e., part of the column constituted by the aromatic parts only) is cylindrical. Therefore, the associated surface area s_{Ar} is circular[16] and equal to $\pi(\Phi_{Ar}/2)^2$, Φ_{Ar} being the diameter of the aromatic part. By using a method recently developed by some of us based on the additivity rule of the partial volumes,[19c] the molecular volume, V_{Mol}, can be written as a sum of the elementary volumes V_{Ar} and V_{Ch} of the aromatic and aliphatic constitutive parts ($V_{Mol} = V_{Ar} + V_{Ch}$). Thus, the volume fraction of the central hard core of the column, *f*, must be V_{Ar}/V_{Mol}.[21b] As s_{Ar} is also equal to *fs*, where *s* is the columnar cross-sectional area, then it is now possible to calculate Φ_{Ar} by using the following relation:

$$\Phi_{Ar} = 2\sqrt{\frac{fs}{\pi}} \qquad (2)$$

With s = 848 Å^2 and V_{Ar} = 630 Å^3,[21] f is evaluated to be 0.25 and the calculated value of Φ_{Ar} is 16.4 Å. The calculated diameter of the hard columnar part (Φ_{Ar}) is therefore slightly smaller than the estimated diameter of the hard core of the disclike molecule, ϕ_{Ar}, which can reflect some orientational fluctuations of the discs with respect to the columnar axis.

To summarize, the columns result from molecular stacking, the driving force of their formation resulting from the antiparallel alignment (Figure 4a) of the planar dipoles (energetically favored arrangement), on one hand, and of $\pi-\pi$ interactions between the large flat aromatic cores, on the other hand. In this alternated stacking, the volume between the branches and between the columns is more efficiently filled by the aliphatic chains. These columns are further packed together in a two-dimensional hexagonal lattice as sketched in Figure 4b. The dipolar interactions and π-overlap between the adjacent rigid conjugated molecular parts contribute to a great extent to the stability of the columnar structure. It is indeed interesting to compare this result with the mesomorphic properties of the structurally related first generation of stilbenoid dendrimers,[22] lacking such permanent dipole. The mesomorphic temperature range is similar, but the clearing point is considerably reduced (≈70 °C). Therefore, compared with the present work, the mesomorphism has been substantially stabilized, thereby supporting our assumption concerning the contribution of the permanent planar dipole to a more optimized stacking (antiparallel stacking) and then to more cohesive columns. The disordered alkyl chains ensured at the same time the gliding of the columns, one with respect to the other, and thus the fluidity and the liquid-crystalline nature of the mesophase.

3.3. Electrochemical Study. In view of the potential application of such molecules in optoelectronics, it is important to consider the relative ionization potential (IP) and electron affinity (EA), parameters that indicate

(21) (a) These values have been estimated from similar investigated systems: see refs 16 and 21b. (b) Marcos, M.; Giménez, R.; Serrano, J. L.; Donnio, B.; Heinrich, B.; Guillon, D. *Chem. Eur. J.* **2001**, *7*, 1006.

(22) (a) Meier, H.; Lehmann, M. *Angew. Chem., Int. Ed.* **1998**, *37*, 643. (b) Meier, H.; Lehmann, M.; Kolb, U. *Chem. Eur. J.* **2000**, *6*, 2462.

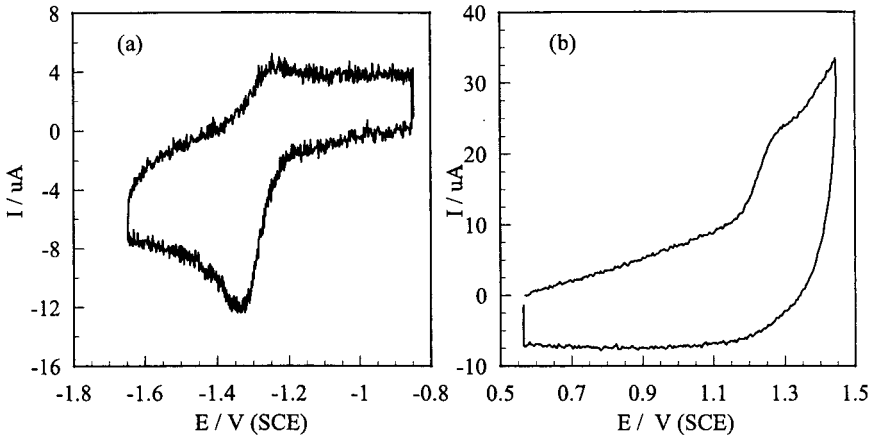

Figure 5. Cyclic voltammetry of **4** in a toluene/acetonitrile mixture (50/50 v/v) containing 0.1 mol L^{-1} NBu_4BF_4 as a supporting electrolyte on a 1-mm-diameter disc glassy carbon electrode: (a) reduction and (b) oxidation voltammograms. Concentration = 1.1 mol·L^{-1}; scan rate = 10 V·s^{-1}; T = 20 °C.

Table 2. Optical and Electrochemical Data of 4 in Dichloromethane and in a Toluene/Acetonitrile Mixture (50/50 v/v), Respectively

optical properties				electrochemical properties[a]	
absorption	emission				
λ_{max} (nm) E_{max} (eV)	λ_{max} (nm) E_{max} (eV)	Stokes shift (nm)	Φ_f (%)	oxidation E_{ox}[b]	reduction E°_{red}
400 *3.1*	550 *2.26*	150	40	1.28	−1.19

[a] Versus SCE (see Experimental Section). [b] Peak potential.

the facility to inject holes and electrons respectively in the material. These values can be estimated from the first oxidation and first reduction potentials in solution, which are associated with the highest occupied and the lowest unoccupied molecular orbitals (HOMO and LUMO energy levels, respectively).[23] For this purpose, the electrochemical behaviors of **4** were investigated by cyclic voltammetry (CV) to measure the redox potentials and thus to estimate IP and EA. Moreover, electrochemical measurements permit us to estimate the chemical stabilities (lifetimes) of the generated ionic species.

The electrochemical oxidation and reduction of **4** have been investigated in a toluene/acetonitrile mixture (50/50 v/v) (see Table 2). This mixture allows good solubility (in the millimolar range in most cases) of the studied compound while keeping a sufficiently high conductivity as required for electrochemical studies. Typical voltammograms of the reduction and oxidation of **4** are presented in parts a and b, respectively, of Figure 5.

In reduction (Figure 5a), the studied compound presents a mono-electronic transfer. The chemical stability of the electrogenerated intermediate can be investigated just by considering the scan rate for which the cyclic voltammogram becomes reversible. The reduction process was reversible at scan rates higher than 10 V s^{-1} (Figure 5a), showing a relatively good chemical stability of the radical anion (lifetime on the order of 1 s). From this reversible voltammogram, the formal potential E°_{red} was immediately derived as the half-sum between the forward and the reverse scan peak potentials[24] (E°_{red} = −1.19 V vs SCE).

In oxidation, only one irreversible process has been observed. This peak remains irreversible even when the scan rate was increased up to several hundred volts per second (Figure 5b), indicating that the lifetime of the produced radical cation is shorter than 1 ms in our experimental conditions. It is noticeable that the radical cation has a much lower chemical stability than the corresponding radical anion. In our determination, the E°_{ox} value (Table 2) was approximated by the corresponding peak potential (E_{ox} = 1.28 V vs SCE).

To a first approximation, the reduction potential can be related to the electron affinity and thus to the LUMO energy level[23] according to the following equation: IP = (E_{ox} + 4.75). The estimated ionization potential ranges in the 6.0 eV region. A similar relationship can be made for the oxidation potential, the ionization potential, and HOMO energies. The calculation shows that **4** possesses a high electron affinity (≈3.6 eV). This value is higher than those previously determined on 6,6′-distyryl-3,3′-bipyridine derivatives[12b] and indicates that electrons could be easily injected in a layer of **4**. It should be noted that the calculated values of the HOMO and LUMO level energies correspond to those determined on a columnar perylene derivative,[11e] which exhibits higher phase transition temperatures.

3.4. Optical Properties in Solution. As a first characterization of the individual molecule (**4**), optical properties were studied in solution. Figure 6 shows the absorption and emission spectra of **4** in dichloromethane; the spectral properties (i.e., absorption and emission maxima, molar extinction coefficient (ϵ), Stokes shift, and quantum yield of fluorescence) are reported in Table 2. It should be noted that no changes of the spectra were observed during repetitive experiments on the same sample, showing that no photochemical reactions (either photoisomerization or photocycloaddition) occur in our experimental conditions.

A single structureless and broad absorption peak is observed at 400 nm (3.10 eV). It is attributed to a $\pi-\pi^*$ transition due to the large molar coefficient absorption (ϵ > 80 000 L mol^{-1} cm^{-1}), indicative of a highly π-conjugated system.

(23) Janietz, S.; Bradley, D. D. C.; Grell, M.; Giebeler, C.; Inbasekaran, M.; Woo, E. P. *Appl. Phys. Lett.* **1998**, *73*, 2453.
(24) Andrieux, C. P.; Savéant, J.-M. Electrochemical Reactions. In *Investigation of Rates and Mechanism of Reactions*; Bernasconi, C. F., Ed.; Wiley: New York, 1986; Vol. 6, 4/E, Part. 2, pp 305−390.

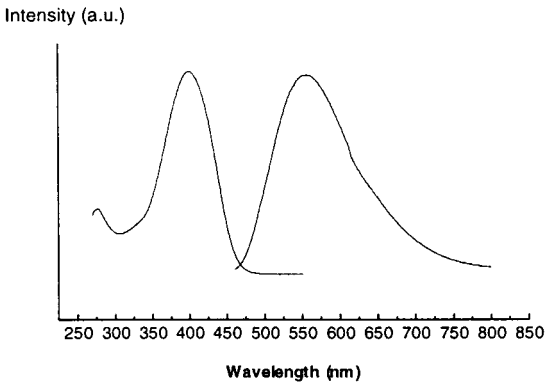

Figure 6. Absorption and emission spectra of **4** in dichloromethane. Intensities of spectra have been normalized to the same value.

The photoluminescence spectrum of **4** results in a broad peak at 550 nm (2.26 eV) with a shoulder around 620 nm (2.00 eV). Additionally, it should be noted that the Stokes shift is on the order of 150 nm. Because the Stokes shift is usually dependent on the structural relaxation of the excited molecule, such a large value (0.84 eV or 1580 cm^{-1}) results from a significant conformational change that occurs upon excitation of **4**. The excited state could be described as being quinoid-like, thus resulting in a planar conformation, and leading to an intramolecular two-dimensional charge-transfer (ICT) state emission (Scheme 2).

4. Conclusion

In conclusion, the design, synthesis, and mesophase characterization of a new class of disclike mesogens containing a permanent dipole have been reported. On the basis of 3,5-dicyano-2,4,6-tristyrylpyridine core, the highly π-conjugated derivatives align in an antiparallel arrangement and form disc-shaped "dimeric" units that self-assemble over a broad temperature range (80−135 °C) into columns themselves packed together in a two-dimensional hexagonal lattice.

In addition, electrochemical as well photophysical properties of the individual disclike molecules have been investigated, in solution. Besides two-dimensional charge transfer and photoluminescence, the electron-accepting character, evidenced by high electron affinity, combined with a columnar self-organization seems promising for electron transport and therefore opens the way to applications in optoelectronics.

The charge transport and optical properties in the liquid-crystalline columnar mesophase are currently in progress. Moreover, because of the versatility of the synthetic pathway, the influence of the strength of the dipolar permanent moment (by varying the nature of the donor group) on mesogenic and electronic properties will also be investigated.

CM010725H